JoT JOURNAL OF TURBULENCE

http://jot.iop.org/

Stationary vortices and persistent turbulence in Karman grooves

Gregory J Balle and Robert E Breidenthal

University of Washington, Seattle, 4617 Sunnyside Avenue N, Seattle, WA 98103, USA
E-mail: balle@aa.washington.edu

Received 22 April 2002
Published 13 August 2002

Abstract. The vortex persistence theory of turbulence predicts that the addition of a stationary vortex will reduce the wall fluxes in turbulent flows. To test the theory, the feasibility of holding a vortex sufficiently stationary whilst embedded in a turbulent boundary layer is investigated. Potential flow analysis reveals that the stationarity of the von Karman street of vortices in a wake might be useful for this purpose. In this scheme, the dividing streamline of the stationary vortex street would be replaced by a solid wall having the same wavy shape, which is given by the derived analytical expression for this streamline. An experimental apparatus with just such a wavy wall was built, including a corotating array of vortex generators that are able to accurately position quasi-streamwise vortices near the stationary points of the wavy wall, i.e. in the 'Karman grooves'. The secondary flow in the cross-plane perpendicular to axes of these vortices corresponds geometrically to that of the vortex street. If the vortices lie exactly upon the geometric stationary points of the Karman grooves, the vortices are observed to be stationary and in the persistent regime of turbulent fluxes. Displacing the vortex generator array only slightly yields different turbulent fluxes. Simple vortex growth measurements provide a graphic demonstration of the difference between persistent and nonpersistent (free) vortices. The experimental set-up was then modified to include a wall heating system and thermocouples to measure the wall heat flux, as a candidate turbulent flux. Experimental results show that the non-dimensional heat transfer coefficient, the Nusselt number, is a function of the Reynolds number with an exponent of $\sim$0.57 if persistent and $\sim$0.82 if nonpersistent. The latter is comparable to the flat plate boundary layer heat flux exponent of $\sim$0.8, for the same Reynolds number range, i.e. 10^4 through 10^5, and the transition between the regimes is observed to be a gradual function of vortex location.

PACS numbers: 47.27.Nz, 47.27.Vf, 44.20.+b

 PII: S1468-5248(02)39791-1 1468-5248/02/000001+18$30.00

Contents

1. Introduction

The persistence theory of turbulence, developed from observations of entrainment rates across a stratified interface, is used to explain the connection between the stationarity of a vortex and its influence on turbulent fluxes across the interface [2, 3]. According to the theory, when a vortex is near an interface, fluxes of scalar quantities at the boundary depend critically upon the stationarity of the vortex, along with other more well known parameters. For a sufficiently strong and stationary vortex, theory predicts that the fluxes will be independent of the fine-scale turbulence. In the limiting case of infinite stratification, i.e. a solid wall, the turbulent fluxes in the influence of a stationary vortex differ widely from the conventional Reynolds number dependencies. Embedding such a stationary vortex in a turbulent boundary layer could theoretically achieve significant reductions in wall heat and momentum transfers, two mechanisms of acute interest to engineers and fluid dynamicists in many fields. In section 2 we give more details on the derivation of the persistence theory of turbulence and how it was used to predict *a priori* the results of the current experiments. However, the driving motivation of this research was to build on the previous results, first by finding a suitable means to hold a vortex stationary near a solid wall and, second by measuring a surface flux, e.g. heat, at the wall near such stationary vortices. Fuller explanations and ramifications of persistent turbulence can be found in the cited references.

The passive control mechanism proposed to hold the vortices stationary in this study is the geometry of the boundary and the vortex array itself. For two-dimensional potential flows with vortex motion, certain configurations of the vortices exhibit stationary points of the vortex path function, i.e. the vortices are at rest when located at these points, [1, 15]. These stationary points can be located near a bounding contour if a suitable streamline is chosen, since in potential flow any streamline can be replaced with a solid wall. There are no such geometric stationary points near a flat wall. Further to this, we have discovered that the well known von Karman vortex street configuration of vortices exhibits the required stationarity properties, and if the dividing streamline of the street is the chosen bounding contour then the construction of an experimental apparatus is relatively simple. In section 3, we derive the exact functionality of the dividing

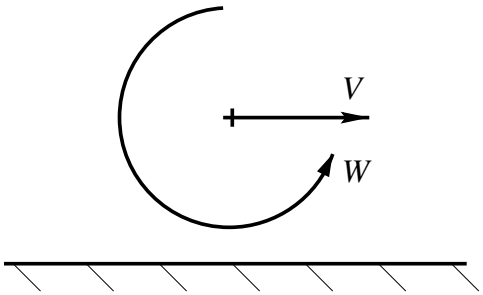

Figure 1. Schematic of a vortex near a boundary.

streamline, enabling a direct comparison with the commercially available sheets with corrugated cross-section such as the one used in these experiments.

Section 4 records the two main areas of experimentation that were carried out. First, simple flow visualization of dyed vortices, located in the Karman grooves, was used as a rudimentary measure of vortex growth, with varying Reynolds number and persistence. This served to give an order of magnitude measure and a check to see if indeed there was anything close to the expected effects taking place. After this had been confirmed, a programme of experimentation for measuring the wall heat flux for persistent and nonpersistent vortices was pursued. Particularly, we were looking to collect data that would enable us to quantify the power law dependency of the Nusselt number, Nu, the non-dimensional heat transfer coefficient, upon the Reynolds number, Re. That is to say, we wanted to measure α for the relation

$$Nu \sim Re^{\alpha}, \tag{1.1}$$

for both the persistent and nonpersistent turbulence regimes.

2. Persistent turbulence

2.1. Background

Recent experiments on stratified entrainment have revealed an important parameter for turbulent fluxes at interfaces, the vortex persistence [3]. These experiments show that the entrainment flux velocity, w_e, non-dimensionalized by the characteristic velocity scale of the turbulence, w_1, is a function of the stationarity, T, or *persistence*, of the entraining eddies. So along with the other more well known parameters, Ri = Richardson number, Pr = Prandtl number, Sc = Schmidt number, and Re = Reynolds number, we have an entrainment law of the form

$$\frac{w_e}{w_1} = f(Re, Ri, Pr, Sc, T). \tag{2.1}$$

Such a relationship would be in the spirit of Taylor's entrainment hypothesis for free turbulent jets [11]. Since T is a measure of vortex stationarity near an interface, we may define this persistence parameter using the ratio of two velocities essential to describing the motion of a vortex near an interface. This ratio is between the translational velocity, V, of the vortex parallel to the boundary and an appropriate measure of the vortex's azimuthal velocity, W, e.g. the local maximum azimuthal velocity (figure 1). The persistence parameter is then simply

$$T \equiv k\frac{W}{V}, \tag{2.2}$$

where k is some constant of proportionality.

If the vorticity structure is of such a chaotic nature as to make impossible the measurement of a representative azimuthal velocity, another scheme would be to use the vortex circulation (an integral quantity) divided by a discernible vortex cross-axis width. The general idea here is to recognize the relative importance of the amplitude of the velocity fluctuation due to the eddy, with respect to its mean motion tangential to the interface. Another point worth noting here is this: while the azimuthal velocity W is unambiguous to any inertial observer, the translational component V is that measured by an observer at rest with respect to the interface. The persistence is thus only well defined for vortices sufficiently near to an interface, such that they can have an influence on the fluxes there.

Among other discoveries made in the experiments mentioned above was the laboratory confirmation of atmospheric measurements showing the turbulent entrainment in a stratified environment to be largely independent of Re and mostly dependent on stratification, Ri. Furthermore, it was found that when a large-scale eddy is brought to rest at the interface, i.e. is persistent, this eddy becomes the dominant entrainment mechanism rather than the usual vortex with eddy Richardson number of unity. In this case, the Ri dependency for the non-dimensionalized entrainment rate changes by a full exponent, i.e.

$$\frac{w_e}{w_1} \sim Ri^{-\frac{3}{2}}$$

for nonpersistent turbulence and

$$\frac{w_e}{w_1} \sim Ri^{-\frac{1}{2}}$$

for persistent turbulence. This successfully explains the seemingly counterintuitive result that a turbulent jet impinging upon a stratified interface produces more entrainment when it is held steady, with its axis perpendicular to the interface, than when it is directed at an angle and/or precessed around [4].

In the current study we are interested in measuring effects in the limiting case of very large Richardson number, $Ri \gg 1$, where stratification drops out of the problem as the interface effectively becomes flat, e.g. a solid wall. We hypothesize, though, that the dependency upon vortex stationarity still holds in this limit [3], where the entrainment, and thus the turbulent fluxes, are dependent upon Re.

2.2. Persistence in the limit $Ri \gg 1$

We may explain this in the following way: fluxes due to a turbulent spectrum near a rigid interface can be given by a surface renewal theory, where mass (via porous diffusion) or another scalar of interest diffuses across the interface and is swept away by eddies of some scale. From dimensional considerations, an effective flux velocity, w_e, is seen to be proportional to the square root of the ratio of the diffusivity, $\mathcal{D}$, divided by a vortex rotation time, i.e.

$$w_e = \left(\frac{\mathcal{D}}{\mathcal{T}_\lambda}\right)^{\frac{1}{2}}, \tag{2.3}$$

where $\mathcal{T}_\lambda$ is the time scale of the rate-limiting eddy in the turbulent cascade. For turbulence with a Kolomogorov spectrum interacting with a solid wall, this time scale is either that of the smallest eddies of length scale λ_0, or that of the largest with length scale δ.

To explain why this should be so, we use the facts that the Kolmogorov eddy (the smallest in the spectrum) has an eddy Reynolds number of 1 and that the flow of energy through the cascade is independent of length scale. From these facts, the ratios of the largest to smallest

length and time scales are then related to the turbulence Reynolds number, Re_δ, by the following relations:

$$\frac{\delta}{\lambda_0} = Re_\delta^{\frac{3}{4}}, \tag{2.4}$$

$$\frac{\mathcal{T}_\delta}{\mathcal{T}_{\lambda_0}} = Re_\delta^{\frac{1}{2}}. \tag{2.5}$$

At large Reynolds numbers the contrast between the largest and smallest eddies becomes obvious. The largest eddies are efficient at transporting large fluid elements large distances as $\delta \gg \lambda_0$, while the smallest eddies are effective at rapidly generating new surface area as $\mathcal{T}_{\lambda_0} \ll \mathcal{T}_\delta$. The intervening inertial subrange merely provides the conduit for transporting a measured scalar to the molecularly mixed interface, wherever it may be located.

When the largest eddies in the spectrum are brought to rest at the interface, i.e. $T \gg 1$, the time scale of the rate-limiting eddy will be that of these stationary vortices, i.e. $\mathcal{T}_\delta$, and the entrainment is said to be in a persistent regime. Conversely, when $T \leq \mathrm{O}(1)$, the time scale of the smallest eddy will be the rate-limiting step, i.e. $\mathcal{T}_{\lambda_0}$, and the entrainment is said to be in the nonpersistent regime. Physically speaking, while the large-scale eddies persist in the same location, i.e. are stationary, the small scales are 'starved' of new fluids to mix at the molecular scale; conversely, when the large scales are 'foraging' along the interface entraining at a much greater rate, the entrained fluid must wait for the smallest eddies to create new interfacial surface area before molecular mixing can occur. In the first case, the overall turbulent flux (entrainment plus mixing) is rate-limited by the time scale of the large, persistent vortices doing the entraining, and in the latter case it is rate-limited by the time scale of the smallest (Kolmogorov) eddies doing the molecular mixing.

With all other factors held constant, e.g. Pr, Sc, and Ri, the difference in the effective flux velocity dependence upon Re at a solid wall between persistent and nonpersistent turbulence is found by simply taking the ratio of the two regimes,

$$\frac{w_{e_N}}{w_{e_P}} = \left[\frac{\mathcal{T}_\delta}{\mathcal{T}_{\lambda_0}}\right]^{\frac{1}{2}} = Re_\delta^{\frac{1}{4}}, \tag{2.6}$$

where subscript N denotes nonpersistent and P persistent. So for any turbulent transfers of a measured scalar of interest we can expect the ratio between the persistent and nonpersistent cases to depend on Reynolds number in this way. In this investigation we are measuring the turbulent heat transfer at a solid wall. Given that this is a process governed largely by the eddy cascade mechanism, we could then expect the non-dimensional heat transfer to obey a functionally similar relationship to that above, i.e.

$$\frac{Nu_N}{Nu_P} \sim Re_\delta^{\frac{1}{4}}, \tag{2.7}$$

Nu_N being the Nusselt number for nonpersistent regimes and Nu_P the Nusselt number for persistent turbulence. This relationship has the reasonable requirement that turbulent heat transfer is a linear function of the effective flux velocity due to the turbulence, in both cases. In section 4.3 we discuss further how the entrainment flux velocity is related to heat transfer for persistent and nonpersistent regimes.

3. Stationary vortices and the Karman vortex street

3.1. Stationary vortex points

In two-dimensional flow analysis the notion of a vortex centroid has been made quite concrete by [15] and others. However, in three dimensions it is not so clear, although a local plane

perpendicular to the vortex lines will possess a local centroid of sorts. For this study we are dealing with mostly axial vortices, perhaps slightly helical, and so a two-dimensional vortex centroid is a useful concept, particularly the motion of the vortices' centroids and their stationary points.

With a suitably defined centroid it is possible to treat a region where the vorticity is distributed in patches, homogeneously or inhomogeneously, as if the whole of the vorticity acted as one entity, analogous to the grouping of mass points about one 'centre of mass' in Newtonian mechanics. This is most useful when considering the exchanges of momentum, and moment of momentum, between the region in consideration and external influences. This is done using Kelvin's methods [6], whereby the properties of impulsive momentum and impulsive moment of momentum can be attributed to the vortex, in the instantaneously equivalent steady flow, so that force and torque calculations can then be performed with the vortex as if it were a solid body interacting with the fluid and its boundaries.

In this way a region of fluid where the vorticity is scattered, but contained within a definite boundary such as in a turbulent flow field, can be treated as if it behaved like one, or perhaps a few, large-scale vortices. This approach is still somewhat valid in three-dimensional turbulence as the smaller scales tend towards isotropic vorticity direction distributions, which cancels out their net reactions for a large enough volume. The large scales are observed to align into anisotropic structures, with definable axes and something like a centroid in local planes perpendicular to these axes. In this light, the turbulence can be treated as identifiable large-scale vortex structures, within which lies a continuous cascade of many scales of eddy size, as is the assumption in 'large-eddy simulation' Navier–Stokes numerical schemes. With this as our context, it is worthwhile to ask the relatively simple question, discounting all the other numerous complexities of the turbulent motion, 'What are the trajectories of the large-scale vortices?'

Furthermore, with the persistence theory predicting a fundamental change in turbulent fluxes with stationary large-scale vortices it is also important to know which configurations of the large scales are stationary, i.e. at rest with respect to boundaries, to the first order of approximation. These questions can be answered quite confidently for many two-dimensional flow situations, using the familiar mathematics of complex potential theory with introduced axial point vortices. Quite simply, for a given complex potential $F(z)$, with accompanying velocity field $\mathrm{d}F/\mathrm{d}z$, a vortex is stationary wherever

$$\left.\frac{\mathrm{d}F}{\mathrm{d}z}\right|_{z=z_v} = 0, \tag{3.1}$$

z_v being the location of the vortex. When the calculation of equation (3.1) is carried out it should be remembered that contributions to the induced velocity at z_v from the vortex in consideration are zero, as a vortex does not induce velocity upon itself except through images.

In the parlance of phase plane analysis, the stationary points of the vortex path function are the fixed points or 'centres' of the motion and the resulting vortex motion is then due to the vortices orbiting these centres or at rest when located at them. This in itself is a useful result as it enables a locally linearized analysis, using a centre manifold theorem with the vortex stationary points comprising the centres, to be used on the problem of the vortex motion. Superimposed upon this motion is the induced velocity field that is consistent with the vortices themselves. It is also worth noting that the integrated pressure forces exerted on the boundary, due to the motion of the vortices, vanish whenever the vortices are located at the stationary points, as can be shown using the Blasius force law of complex analysis.

There are many configurations of axial vortices that are stationary, perhaps the most simple being that of a single vortex located at the centre of a circular streamline [1]. This suggests that many simple closed contours, with a net circulation in the interior, will contain within them a stationary point of the vortex path function, as many simple closed contours, and thus

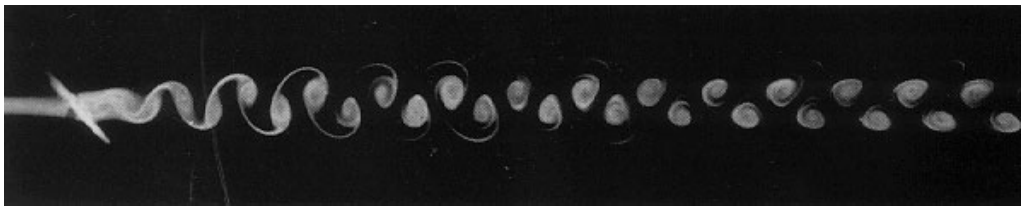

Figure 2. Vortices in the wake of a cylinder; the 'Karman vortex street' [17].

their interior flow fields, can be mapped to the unit circle using the familiar conformal maps of complex variable analysis.

Another class of vortex flows exhibiting stationary points are those associated with unbounded periodic arrays of vortices, the most simple of which is the stationary single row of equidistant vortices extending to infinity, the mathematical idealization of Lord Rayleigh's well known plane vortex stratum (the planar shear layer), containing within it Kelvin's 'cat's-eyes' vortices [7]. Then there is the double row of vortices, where each row has an opposite sense of rotation, this being a mathematical idealization for jets and wakes [10]. A well-studied stationary configuration for the double-row array is where the vortices of one row lie adjacent to the midpoint between the vortices of the other row, commonly known as the 'von Karman vortex street.'

3.2. Karman's stationary vortex street

Many studies, [5, 8, 12, 16] to name but a few, have explored this flow (figure 2), particularly the question of the absolute two-dimensional stability, in cases including viscous fluids and finite-diameter vortices. von Karman's result for infinitesimal line vortices in an irrotational fluid yields the simple mathematical relationship governing the dimensions of what he called the stable array,

$$\sinh \frac{\pi h}{a} = 1, \tag{3.2}$$

with useful alternate forms

$$\cosh \frac{\pi h}{a} = \sqrt{2} \qquad \text{and} \qquad \frac{h}{a} = \frac{\ln(1+\sqrt{2})}{\pi},$$

where h is the distance between the staggered rows of vortices and a is the distance between adjacent vortices in a row. An analysis by [10] expands and verifies this result; however, later Liupanov-type approaches in [9] and others call into question the absolute stability. Although the wealth of mathematical stability analyses performed on this flow state are informative, they are not necessary in identifying that the von Karman vortex street is indeed a *stationary* solution of the vortex motion. Also, the growth of the instabilities seems to be intimately linked with the growth of the vortices themselves in turbulent wakes [13, 14], and the underlying stationary solution would seem to play an integral role in determining the size of the instabilities.

Given that we know an array of vortices with the spacing geometry of equation (3.2) is stationary, we propose to use one row of this configuration as a mechanism to embed a corotating array of stationary vortices within a turbulent, solid-wall boundary layer, this being a prerequisite for achieving a persistent regime of turbulence near the solid-wall interface, as described in section 2. The most obvious streamline to chose as our solid wall would then be the dividing streamline of the street (see bold curve in figure 3); this is mathematically identical to having an image system of vortices positioned relative to the physical vortices so as to complete the stationary Karman street.

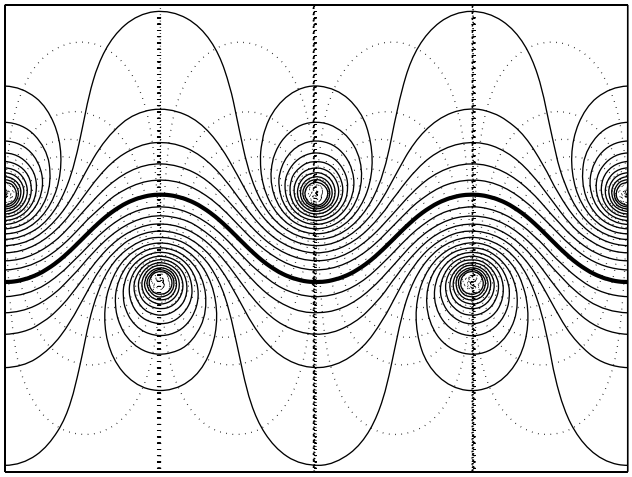

Figure 3. Streamlines of the Karman vortex street, dividing streamline in bold.

In this set-up, the largest component of the freestream flow is parallel with the axes of the vortices, although it is necessary to have precisely the right component perpendicular to the axes, to bring the vortices to rest with respect to the wavy wall (as explained in section 3.3). The resulting experimental rig, with the dividing streamline of the Karman street as its cross-section, is then simply a grooved plate with a corotating vortex generator array positioned at the upstream end of the Karman grooves. For the vortices to be stationary the vortex generators need to be positioned precisely so that the resulting tip vortices lie in the centre of the grooves and on the plane tangent to the centre of the grooves and on the plane tangent to the ridges, not really down in the hollows. Again, see figure 3 for the locations of the stationary vortices.

3.3. Dividing streamline of Karman vortex street

In order to construct an apparatus having Karman grooves, it was necessary to calculate the shape function of the dividing streamline of the Karman vortex street. The complex potential for the vortex street with vortices of strength Γ is given by

$$F(z) = -\frac{\mathrm{i}\Gamma}{2\pi}\left[\ln\left(\sin\frac{\pi}{a}\left(z - \mathrm{i}\frac{h}{2}\right)\right) - \ln\left(\sin\frac{\pi}{a}\left(z - \frac{a}{2} + \mathrm{i}\frac{h}{2}\right)\right)\right]. \tag{3.3}$$

This result is derived from an infinite array of counter-rotating vortices as outlined in, for example [15]. However, the potential given above has the origin shifted from being located at a singularity; this avoids problems associated with the conjugate mapping dealing with an asymmetrically positioned array, the conjugate mapping being an implicit part of streamfunction calculations. Using the sine sums of angles formula this can be expanded and then we collect terms inside a single log function as follows:

$$F(z) = -\frac{\mathrm{i}\Gamma}{2\pi}\ln\left[\frac{A_1 + \mathrm{i}B_1}{A_2 + \mathrm{i}B_2}\right],$$

where

$$A_1 = \cosh\frac{\pi}{a}\left(y - \frac{h}{2}\right)\sin\frac{\pi x}{a}, \qquad B_1 = \sinh\frac{\pi}{a}\left(y - \frac{h}{2}\right)\cos\frac{\pi x}{a},$$

$$A_2 = \cosh\frac{\pi}{a}\left(y + \frac{h}{2}\right)\sin\frac{\pi}{a}\left(x - \frac{a}{2}\right), \qquad B_2 = \sinh\frac{\pi}{a}\left(y + \frac{h}{2}\right)\cos\frac{\pi}{a}\left(x - \frac{a}{2}\right).$$

Now, we get the streamfunction for the vortex street, Ψ, in a compact form by using $\mathrm{i}\Psi = \frac{1}{2}[F(z) - F^*(z)]$ [1]:

$$\Psi(x,y) = -\frac{\Gamma}{4\pi}\ln\left[\frac{A_1^2+B_1^2}{A_2^2+B_2^2}\right] = -\frac{\Gamma}{2\pi}\ln\frac{R_1}{R_2}, \tag{3.4}$$

where

$$R_1^2 = A_1^2 + B_1^2 = \sinh^2\frac{\pi}{a}\left(y-\frac{h}{2}\right) + \sin^2\frac{\pi}{a}x,$$
$$R_2^2 = A_2^2 + B_2^2 = \sinh^2\frac{\pi}{a}\left(y+\frac{h}{2}\right) + \cos^2\frac{\pi}{a}x.$$

As an aside, we can use a similar method to obtain an expression for the potential function of x and y. It is the conjugate harmonic function of the stream function and is comprised of an orthogonal family of curves, given by

$$\Phi(x,y) = \frac{1}{2}[F(z) + F^*(z)] = \frac{\Gamma}{2\pi}(\Theta_1 - \Theta_2), \tag{3.5}$$

where

$$\tan\Theta_1 = \frac{B_1}{A_1} = \frac{\tanh\frac{\pi}{a}(y-\frac{h}{2})}{\tan\frac{\pi x}{a}}, \qquad \tan\Theta_2 = \frac{B_2}{A_2} = \frac{\tanh\frac{\pi}{a}(y+\frac{h}{2})}{\tan\frac{\pi}{a}(x-\frac{a}{2})},$$

plotted as the dotted curves on figure 3.

The dividing streamline has $\Psi = 0$ and can be derived from equation (3.4) to give the implicit expression in x and y for any aspect ratio of the street,

$$\cos\frac{2\pi x}{a} + \sinh\frac{\pi h}{a}\sinh\frac{2\pi y}{a} = 0.$$

The Karman condition for a stationary array, i.e. $\sinh\frac{\pi h}{a} = 1$, may then be used to obtain the dividing streamline for the stationary array as the remarkably simple expression

$$\cos\frac{2\pi x}{a} + \sinh\frac{2\pi y}{a} = 0, \tag{3.6}$$

which can also be written explicitly for y as

$$y = \frac{a}{2\pi}\ln\left[\sqrt{1+\cos^2\frac{2\pi x}{a}} - \cos\frac{2\pi x}{a}\right]. \tag{3.7}$$

Note that this is a purely geometric relationship, independent of the circulation strength of the vortices. We have plotted this relation in bold on the same graph with a plot of the streamlines and potential function, see figure 3. This then is the shape of the boundary required to bring the vortices to rest when located at the stationary points of the vortex path function and our experimental apparatus should have a shape cross-section as close as possible to this.

There is one further piece to the puzzle that should be noted. By examining the velocity of translation of any one of the vortices of the street, with respect to the fluid at rest at infinity, it is seen that the whole street moves with a velocity

$$U_{street} = \frac{\Gamma}{2a}\tanh\frac{\pi h}{a}. \tag{3.8}$$

Therefore, in order to bring to rest the complete vortex street, with respect to the plate, we need to introduce a cross-flow component by yawing the plate relative to the freestream such that this component cancels exactly the velocity of propagation given in equation (3.8), see figure 4.

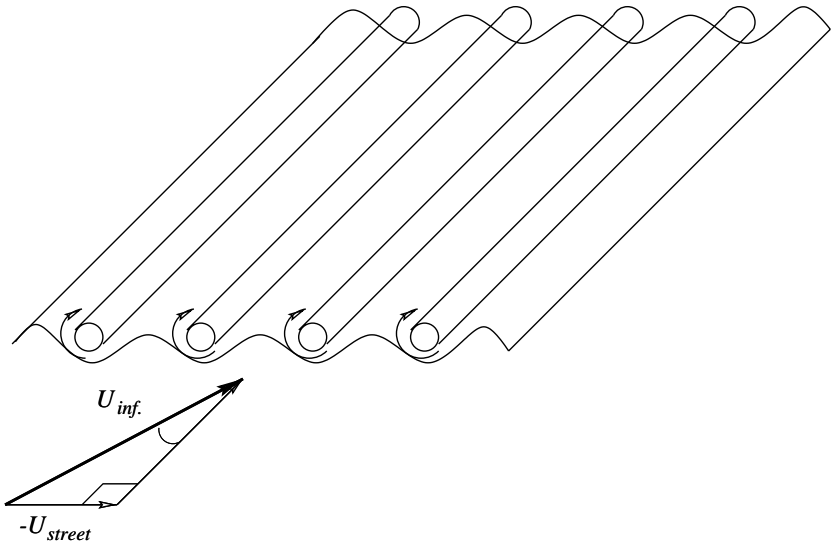

Figure 4. Schematic of the Karman grooved plate with stationary vortices and freestream cross-flow component due to plate yaw.

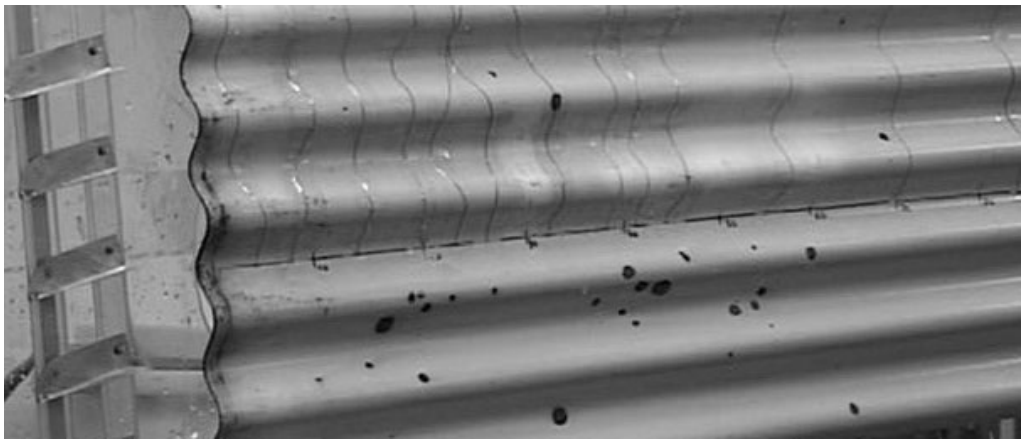

Figure 5. Photograph of experimental apparatus.

The exact velocity component is found by substituting the Karman condition for the stationary street into equation (3.8), so the cross-flow velocity must be set equal to

$$U_{street} = \frac{\Gamma}{2\sqrt{2}a}. \tag{3.9}$$

In this way the vortex motion and accompanying induced velocity field are consistent with the freestream motion and the boundary being at rest in the laboratory frame.

4. Experiments

4.1. Apparatus

A photograph of the experimental apparatus is shown in figure 5. The major components seen are the corrugated metal sheet and the corotating array of vortex generators mounted upon a translatable sliding mechanism on the left (upstream); this in turn is mounted on a short leading

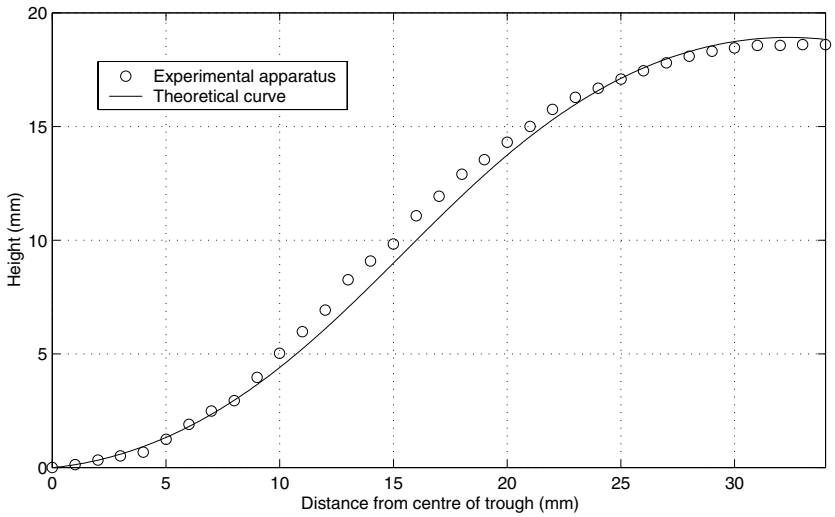

Figure 6. Plot of actual and theoretical shape cross-sections, 1/2 wavelength shown.

edge plate. With this arrangement, the initial vortex position relative to the stationary point could be adjusted. Not seen in the photograph is the heater mounted to the backside of the plate, encapsulated in insulating foam. This apparatus was submerged in a water tunnel with 70 cm × 70 cm cross-section, a maximum flow speed of 70 cm s^{-1}, and background turbulence level less than 0.2%.

Fortuitously, a conventional prefabricated sheet of corrugated roofing material with an aspect ratio of the corrugations very close to the Karman condition was found to be available. It is an old standard with dimensions $a = 22/3$ inches (67.73 mm) by $h = 3/4$ inches (19.05 mm) yielding $h/a = 0.2812$ (versus $h/a = 0.2805$ for the theoretical value from equation (3.2)), the new standard being shallower to save material. The actual shape of the corrugated surface is approximately equal to the shape of the dividing streamline of the Karman vortex street, given by equation (3.6). In figure 6 we have plotted the shape of one-half wavelength of the actual surface taken from measurements with a dial micrometer, along with the actual calculated shape of equation (3.7).

The vortex generators (VGs) were of a simple half-delta wing type; these are very similar to those used for 'energizing the boundary layer' to delay high angle of attack separation in aerospace applications. The VG array could be translated as one and the angle of attack of the VGs was also adjustable in situ via a screw mechanism. The circulation generated by a single such delta wing device can be estimated from thin airfoil theory found in the standard texts,

$$\Gamma = \pi \alpha L U_{inf}, \tag{4.1}$$

where Γ = circulation, U_{inf} = freestream velocity, L = length scale of the wing, and α is the local angle of attack of the wing. The angle of attack, α, is made up of the flow component due to the angle of the VG relative to the plate plus a component due to the yaw angle of the plate,

$$\alpha = \alpha_{pl} + \alpha_{vg}. \tag{4.2}$$

So that the vortices are at rest in the reference frame of the plate, the yaw angle of the plate must be related to the freestream velocity by

$$\sin \alpha_{pl} = \frac{U_{street}}{U_{inf}}. \tag{4.3}$$

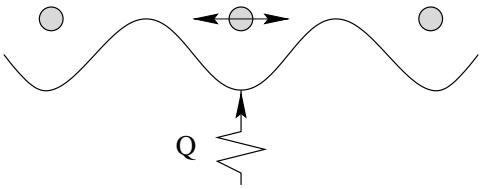

Figure 7. Schematic of plate heating system and translatable vortices.

Recall that the circulation is related to the velocity of the street through equation (3.9). With the spanwise length scale of the VG being set equal to h, the amplitude of the wavy wall, we can be sure that the tip vortex of the delta wing is close to the stationary point height associated with the wall. Also, this leads to the simple expression relating α_{pl} to α_{vg} for small yaw angles of the plate where $\sin \alpha_{pl} \approx \alpha_{pl}$,

$$\alpha_{vg} = \left(\frac{2\sqrt{2}}{\ln(1+\sqrt{2})} - 1 \right) \alpha_{pl}, \tag{4.4}$$

using equations (3.9)–(4.2), and the Karman condition. We must keep in mind here that since the VGs are attached with their span perpendicular to the wall, they are partially submerged within the wall boundary layer and so cannot be expected to generate exactly the lift, and hence circulation, that one would expect from an unbounded wing. For all the heat transfer measurements presented in this paper, $\alpha_{pl} = 5^\circ$ and $\alpha_{vg} \approx 10^\circ$.

The heater component was of a silicone strip type capable of producing 1.55 W cm^{-2} and was affixed to the backside (the side opposite the vortex flow) of the plate. See figure 7 for a schematic of a cross-section of the apparatus depicting heater element and adjustable vortex position. Surrounding this heater was a 3–4 cm thick layer of insulating foam ensuring that the bulk of the heat transfer was through the plate and into the external flow of interest. This heating system was able to provide up to 10 °C difference between the wall temperature and the ambient water temperature. A system of thermocouples for measuring wall temperature was attached to surface of the plate, along the central line in the valley of one of the grooves. A separate thermocouple measured ambient temperature of the water tunnel; these thermocouples have an accuracy of ±0.003 °C.

4.2. Turbulent vortex growth

With the apparatus submerged in a water tunnel, dye was bled into the flow near the apex of the vortex generators to visualize the path and width of the vortex. This was done using both LIF (laser induced fluorescence) type dye and regular vegetable dye with strong backlighting. Digital video camera photography allowed for an analysis of many good quality still frames (up to 30 s^{-1}) and a variable electronic shutter speed enabled a rudimentary averaging over the small-scale fluctuations.

The envelope of the dye was taken as proportional to the vortex growth and measured for several flow speeds. Since the dye traces particle paths rather than streamlines, we are measuring only the envelope of the dye location rather than attempting to track individual vortex lines. In this way we expect to garner some approximate information on the size of the vortex at different downstream locations. Figure 8 is a representative photograph of the comparison between a vortex with a cross-plane position near the stationary point of a Karman groove (bottom photo) and an identical vortex (same vortex circulation and flow speed) adjacent to a flat plate (top

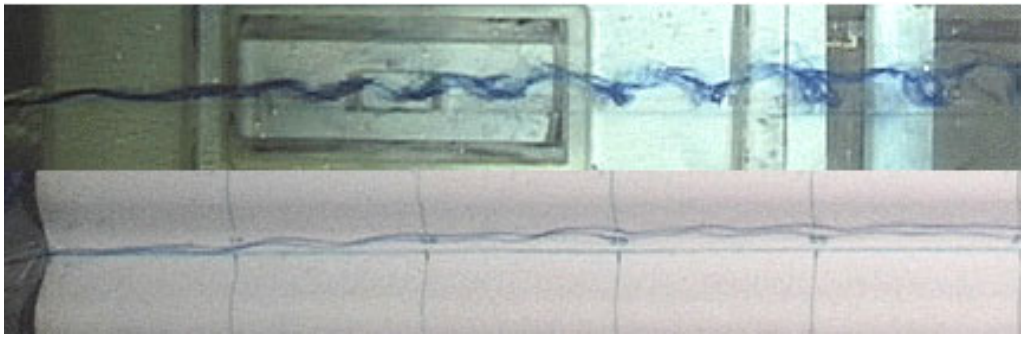

Figure 8. Plan view of dye-traced vortices; flat plate (top), grooved (bottom).

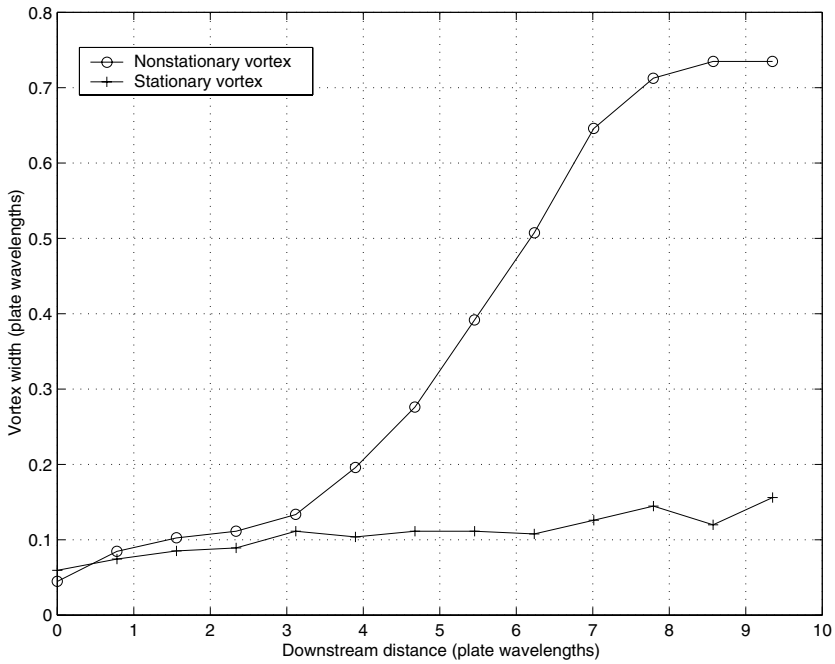

Figure 9. Non-dimensional plot of vortex width versus downstream distance; $Re_a \approx 7100$.

photo). In the figure the Reynolds number was about 7100 based on plate wavelength, a, and the same length of plate is displayed in each case.

As is evident in figure 8, the growth of instabilities, hence the growth of the vortex itself, in the flat plate case far exceeds that of the vortex in the Karman grooves case, for the length of plate of interest. This was shown to be the same for the several other flow speeds observed and it was concluded that the behaviour of these vortices, when placed near a boundary with a such a geometry, is qualitatively different from that of the vortex near a flat wall. To the accuracy of these basic measurements, the growth of the vortices is also quantitatively different, as is evidenced by figure 9; this shows the vortex width versus downstream distance, both non-dimensionalized by plate wavelength. This width corresponds to the envelope of the dye traces in the photographs of figure 8 for the flat plate and for the grooved one.

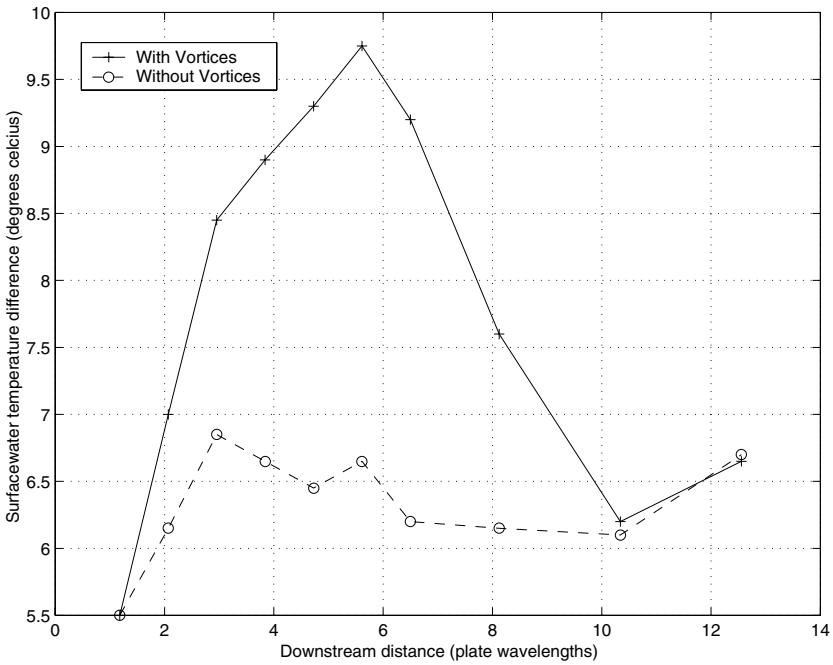

Figure 10. Change in ΔT due to stationary vortices, $Re_a \approx 22\,500$.

4.3. Turbulent fluxes

With the experimental confirmation that these vortices behave qualitatively differently than those near a flat plate, the next step involved measuring a turbulent flux at the surface for both a nonstationary and a stationary vortex. This, according to the theory, should give rise to a difference in the turbulent flux regimes, with the difference between persistent and nonpersistent regimes being a predictable factor. To observe this difference we chose to measure the heat flux at the surface of the Karman grooves plate for the two regimes. The apparatus for generating and measuring a temperature difference between the grooved plate and the external flow is described in section 4.1.

With the temperature difference comes a convected heat transfer; the local flux of this transfer may be expressed using Newton's law of cooling,

$$q_x = h_x(T_s - T_\infty), \tag{4.5}$$

where q_x = local heat flux, h_x = local convection coefficient, T_∞ = temperature of external flow, and T_s = temperature of the surface. The local flux is derived by applying Fourier's law to the fluid at the wall, i.e.

$$q_x = -k_f \left.\frac{\partial T}{\partial y}\right|_{y=0}, \tag{4.6}$$

where k_f is the conductivity of the fluid. Combining equations (4.5) and (4.6) yields

$$h_x = \frac{-k_f \partial T/\partial y|_{y=0}}{T_s - T_\infty}. \tag{4.7}$$

The Nusselt number of non-dimensionalized heat transfer, based on downstream distance, x, is then obtained using h_x, k_f, and x,

$$Nu_x = \frac{h_x x}{k_f}. \tag{4.8}$$

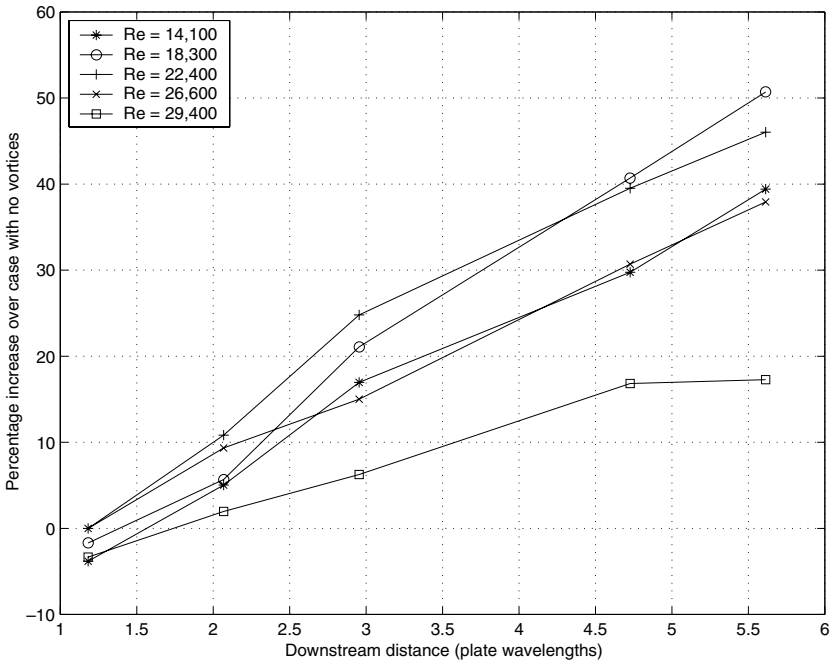

Figure 11. Change in ΔT due to stationary vortices (as percentage of case without vortices).

The Nusselt number may also be written as a function of w_e. To do this we begin with a dimensional argument for the heat flux:

$$\frac{q_x}{\Delta T} = \rho C_p w_e, \tag{4.9}$$

where ρ = mass density of the fluid, C_p = specific heat capacity, and $\Delta T = T_s - T_\infty$; we then use equation (4.5) to get $h_x = \rho C_p w_e$ and so

$$Nu_x = \frac{\rho C_p w_e x}{k_f}. \tag{4.10}$$

The ratio of nonpersistent heat transfer to persistent heat transfer is then simply

$$\frac{Nu_N}{Nu_P} = \frac{w_{eN}}{w_{eP}} = Re_\delta^{\frac{1}{4}}, \tag{4.11}$$

since all other factors are constant, and this provides the promised explanation of equation (2.7).

With our heater generating close to homogeneous 0.62 W cm^{-2} (operating at 40% power levels) the heat flux is actually independent of x, i.e. $q_x \approx$ const. This means that h_x from equation (4.7) is dependent only upon the surface-water temperature difference, ΔT. What we are really interested in here then is the change in ΔT, when we have the persistent vortices and when we do not. So, first we plot ΔT for these two cases to demonstrate the radical change taking place in the heat transfer due to the introduction of the vortices.

Figure 10 shows ΔT as a function of downstream difference, plotted at a representative flow speed. The upper curve is for the case when the persistent vortices are present, the lower is when they are not. Remarkably, although in accordance with the theory, the surface-water temperature difference *increases* with the introduction of the stationary vortices. At the downstream location of about 6 wavelengths this trend is lost; the change in the trend is consistent with where the vortices were seen to leave the stationary location and rapidly grow (within 1–2 wavelengths).

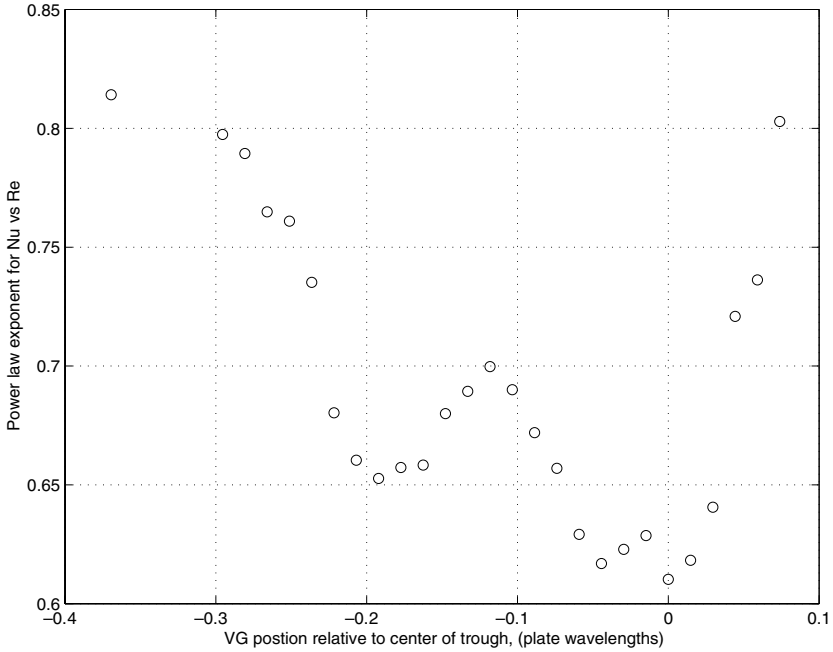

Figure 12. Power law exponent for Nu_x versus Re_x as function of vortex position.

Also note that as a percentage, the case with the vortices has up to a 50% increase in temperature difference over the case without the vortices.

In figure 11 we plot the percentage increase in temperature difference for various flow speeds, i.e. we plot

$$\frac{\Delta T_{vg} - \Delta T_{novg}}{\Delta T_{novg}} \qquad \text{versus } \frac{x}{a}, \tag{4.12}$$

where ΔT_{vg} denotes temperature difference for persistent vortices and ΔT_{novg} the case with no vortices. On this plot we have also eliminated the points downstream of the location where the vortices are observed to leave the stationary location.

We next gathered data measuring the temperature difference and with use of equation (4.8) evaluated the slope of log–log plots of Nu_x versus Re_x. This slope gives us the exponent of equation (1.1), α, and it was calculated for various positions of the VG as it was moved across the location of the stationary point. Figure 12 shows the Nu_x versus Re_x exponent plotted for each position of the VG. Clearly, there is a marked change in the heat transfer properties as the vortex is moved a relatively small distance (less than one-third of a wavelength), and the power law exponent achieves a minimum at the point when the vortex is located closest to the stationary point. When the vortex is moved away from the stationary point, the turbulent transfers approach the expected power law of a 'free' nonpersistent turbulent boundary layer (α is about 0.8 for this range of Re).

Interestingly, we see an asymmetry in figure 12 which indicates that the persistent turbulent regime collapses more rapidly when the vortex is moved in one direction than in the other. This is consistent with the fact that the induced velocity field of a vortex translated away from a stationary point will not be symmetric. The vortex path is similarly unsymmetric: if the vortex begins to one side of the stationary point, the vortex path is down and back towards the stationary point; if it begins the other side, the vortex path is up and out into the free stream. The direction of asymmetry in the data is consistent with this notion and the actual rotational

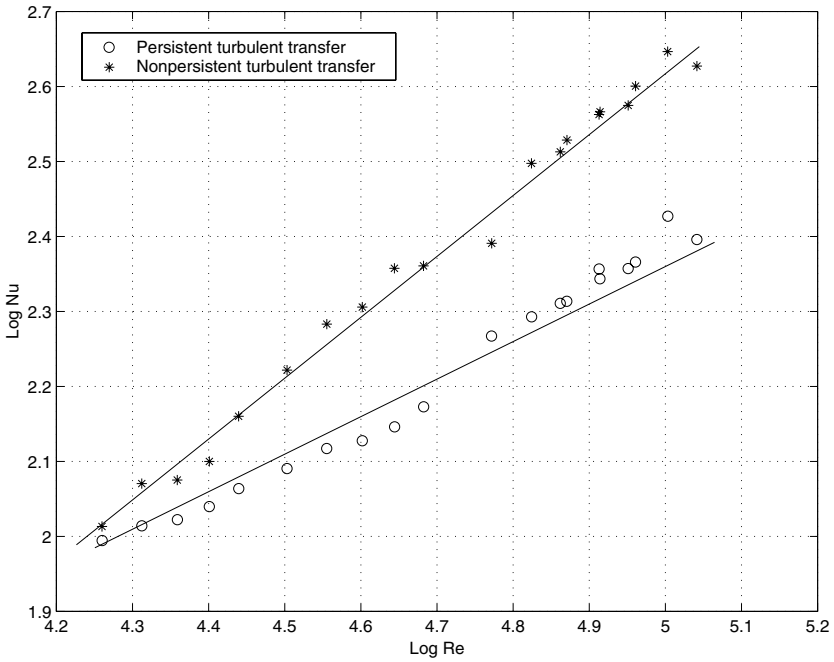

Figure 13. Log Nu_x versus log Re_x for persistent and nonpersistent turbulence.

sense of the vortex. Figure 12 also raises the question of what could give rise to the second minimum of heat transfer that occurs at around 1/5 of a wavelength from the stationary point. Perhaps (and this is mere speculation) a stationary helical mode of the vortex could trigger another regime of persistence.

Experimentally, we were able to achieve stationary vortices for numerous α_{vg} and α_{pl} combinations. Further to this though, we wanted to find the power law difference, as described in equation (2.7). For this we needed a dimensionally similar nonpersistent case for comparison, and the flat plate case is geometrically fundamentally different from a wavy wall. Clearly, for a good comparison between persistent and nonpersistent turbulent fluxes the only thing that should be varied is the persistence parameter, which can be achieved by varying only the initial location of the vortices. Figure 12 shows that the transition between the persistent and nonpersistent regimes is rather gradual and for this reason we chose a position sufficiently far away from the persistent 'sweet spot' so that a good comparison could be made.

Figure 13 shows the results of the comparison. Log Nu_x is plotted versus log Re_x for the two cases, persistent and nonpersistent. A least squares best fit for straight lines puts the slope of the upper line (nonpersistent) at 0.8293 and that of the lower line (persistent) at 0.5752. This is in accordance with the decline in turbulent fluxes by an order of $Re^{\frac{1}{4}}$ expected from equation (2.7), since $0.8293 - 0.5752 = 0.2541 \approx 1/4$.

5. Conclusions

In this paper we have described a new method for the control of turbulent wall fluxes. Vortices placed at stationary points near a wavy wall were shown to affect the turbulent flux of heat at the surface. According to the theory of vortex persistence, the wall flux under such stationary vortices should enter the persistent regime of turbulent fluxes and decline by a factor of $Re^{\frac{1}{4}}$, compared to the nonpersistent case. Preliminary experimental measurements were in accordance with the theory. We have also shown that the fluxes are a strong function of the vortex's initial

position relative to the stationary points. Future work might include the determination of the threshold vortex strength and further investigation of the stationarity characteristics required to achieve the persistent regime of turbulent fluxes.

Acknowledgments

We would like to acknowledge the work of Helmi Touel and Xavier Marduel (both from Ecole Polytechnique, Palaiseau) and Thiemo Kier (University of Stuttgart) in assisting with experimental aspects of this project. Also the encouragement and editing skills of Patricia Burgess were much appreciated.

References

[1] Balle G J 2001 Stationary vortices and persistent turbulence *PhD Thesis* University of Washington, Seattle
[2] Breidenthal R E 1999 Turbulent stratified entrainment and a new parameter for surface fluxes *Recent Research Developments in Geophysics* vol 2, ed S G Pandalai pp 61–65 (Research Signpost)
[3] Cotel A J and Breidenthal R E 1997 A model of stratified entrainment using vortex persistence *Appl. Sci. Res.* **57** 349
[4] Cotel A J, Gjestvang J A, Ramkhelawan N N and Breidenthal R E 1997 Laboratory experiments of a jet impinging on a stratified interface *Exp. Fluids* **23** 155–60
[5] Domm U 1956 Uber Wirbelstrassen von geringster Instabilitat *Z. Angew. Math. Mech.* **36** 367
[6] Kelvin, Lord (Thomson, William T) 1868 On vortex motion *Trans. R. Soc. Edinburgh* **25** 217–60 (Also: *Collected Works* **IV** 13–65)
[7] Kelvin, Lord (Thomson, William T) 1880 On a disturbing infinity in Lord Rayleigh's solution for waves in a plane vortex stratum *Nature* **23** 45–6 (Also: *Collected Works* **IV** 186–7)
[8] Kida S 1982 Stabilizing effects of finite core in a Karman vortex street *J. Fluid Mech.* **122** 487
[9] Kochin N E, Kibel I A and Roze N V 1964 *Theoretical Hydrodynamics* (New York: Interscience)
[10] Lamb H R 1932 *Hydrodynamics* (New York: Dover) Article 156
[11] Morton B R, Taylor G I and Turner J S 1956 Turbulent gravitational convection from maintained and instantaneous sources *Proc. R. Soc.* A **234** 1–23
[12] Meiron D I, Saffman P G and Schatzman J C 1984 The linear two-dimensional stability of inviscid vortex streets of finite-cored vortices *J. Fluid Mech.* **147** 187–212
[13] Roshko A 1953 On the development of turbulent wakes from vortex streets *NACA Tech. Note* 2913
[14] Roshko A 1993 Instability and turbulence in shear flows *Theoretical and Applied Mechanics IUTAM* (Amsterdam: Elsevier Science)
[15] Saffman P G 1992 *Vortex Dynamics* (Cambridge: Cambridge University Press) ch 7
[16] von Karman Th 1911 Uber den Mechanismus des Widerstandes, den ein bewegter Korper in einer Flussigkeit erfahrt *Gottinger Nachrichten Math. Phys. Klasse* 509
von Karman Th 1911 Uber den Mechanismus des Widerstandes, den ein bewegter Korper in einer Flussigkeit erfahrt *Gottinger Nachrichten Math. Phys. Klasse* 547
[17] Zdravkovich M M 1969 Smoke observations of the formation of a Karman vortex street *J. Fluid Mech.* **37** 491–6